BIOCHEMISTRY
including biophysical chemistry & molecular biology
Article

*Biochemistry* **2011,** *50,* 1641–1650 1641
DOI: 10.1021/bi101678a

# Uptake, Distribution, and Speciation of Selenoamino Acids by Human Cancer Cells: X-ray Absorption and Fluorescence Methods[†]

Claire M. Weekley,[‡] Jade B. Aitken,[§] Stefan Vogt,[∥] Lydia A. Finney,[∥] David J. Paterson,[⊥] Martin D. de Jonge,[⊥] Daryl L. Howard,[⊥] Ian F. Musgrave,[@] and Hugh H. Harris*[,‡]

[‡]*School of Chemistry and Physics, The University of Adelaide, Adelaide, SA 5005, Australia,* [§]*School of Chemistry, The University of Sydney, Sydney, NSW 2006, Australia,* [∥]*X-ray Science Division, Argonne National Laboratory, Argonne, Illinois 60439, United States,* [⊥]*Australian Synchrotron, Clayton, VIC, Australia, and* [@]*School of Medical Sciences, The University of Adelaide, Adelaide, SA 5005, Australia*

*Received October 19, 2010; Revised Manuscript Received January 19, 2011*

ABSTRACT: Selenium compounds exhibit chemopreventative properties at supranutritional doses, but the efficacy of selenium supplementation in cancer prevention is dependent on the chemical speciation of the selenium supplement and its metabolites. The uptake, speciation, and distribution of the common selenoamino acid supplements, selenomethionine (SeMet) and *Se*-methylselenocysteine (MeSeCys), in A549 human lung cancer cells were investigated using X-ray absorption and fluorescence spectroscopies. X-ray absorption spectroscopy of bulk cell pellets treated with the selenoamino acids for 24 h showed that while selenium was found exclusively in carbon-bound forms in SeMet-treated cells, a diselenide component was identified in MeSeCys-treated cells in addition to the carbon-bound selenium species. X-ray fluorescence microscopy of single cells showed that selenium accumulated with sulfur in the perinuclear region of SeMet-treated cells after 24 h, but microprobe selenium X-ray absorption near-edge spectroscopy in this region indicated that selenium was carbon-bound rather than sulfur-bound. X-ray absorption and X-ray fluorescence studies both showed that the selenium content of MeSeCys-treated cells was much lower than that of SeMet-treated cells. Selenium was distributed homogeneously throughout the MeSeCys-treated cells.

Selenium is an essential element, which at supranutritional doses has been linked to reductions in cancer incidence and mortality. The seminal study in this field, The Nutritional Prevention of Cancer (NPC)[1] Trial, showed that supplementation of 200 $\mu$g of Se/day as selenized yeast led to significant reductions in total cancer incidence and mortality and in the incidence of prostate cancer (*1*, *2*). A more recent study, the Selenium and Vitamin E Cancer Prevention Trial (SELECT), investigated cancer risk associated with supplementation of 200 $\mu$g of Se/day as selenomethionine (SeMet), vitamin E, or a combination of both. The trial ceased 7 years into a planned 12-year study as there was no evidence of any benefit from either SeMet or vitamin E supplementation, but a small nonsignificant increase in the incidence of type 2 diabetes was observed in subjects taking only SeMet supplements (*3*). Selenized yeast tablets from the manufacturer of the NPC Trial tablets have been shown to have highly variable SeMet content (18−69%), with three other significant components remaining unidentified (*4*). The biological activity of Se is dependent on the chemical form of the Se compound, and it has been hypothesized that it is the methylated metabolites of Se supplements that are largely responsible for the anticancer properties of Se (*5*). As different Se compounds follow different metabolic pathways (*6*), the contradictory results of the NPC Trial and SELECT may be related to the use of different forms of Se supplementation. There is a clear need to identify the metabolites of different Se compounds in vivo to determine the most efficacious form of Se supplementation in cancer prevention.

The selenoamino acids, selenomethionine (SeMet) and *Se*-methylselenocysteine (MeSeCys), occur naturally in foods, are available as nutritional supplements, and have both been investigated for their anticancer properties (*7*). There are key differences between the metabolic pathways of these selenoamino acids and those of free selenide (formally $HSe^-$), the postulated cellular storage form of Se (*8*−*10*). SeMet can be adventitiously incorporated into proteins as SeMet or metabolized to selenocysteine (SeCys) and then lysed to $HSe^-$ by $\beta$-lyase (*11*). SeMet may also be cleaved directly to MeSeH by $\gamma$-lyase (*12*). MeSeCys is not directly incorporated into proteins but is known to undergo cleavage by $\beta$-lyase to MeSeH, thereby largely avoiding metabolism to $HSe^-$ (*13*). MeSeH is a putative generator of reactive oxygen species, and the ability of MeSeCys to produce MeSeH more efficiently than SeMet is thought to make MeSeCys a more effective chemopreventative agent (*9*).

[†]This research was supported under the Australian Research Council's Discovery Projects funding scheme (DP0984722 and DP0985807, QEII). We acknowledge travel funding provided by the International Synchrotron Access Program (ISAP) managed by the Australian Synchrotron. The ISAP is an initiative of the Australian Government being conducted as part of the National Collaborative Research Infrastructure Strategy.

*To whom correspondence should be addressed. Telephone: +61-8-8303-5060. Fax: +61-8-8303-4358. E-mail: hugh.harris@adelaide.edu.au.

[1]Abbreviations: NPC, Nutritional Prevention of Cancer; SELECT, Selenium and Vitamin E Cancer Trial; SeMet, selenomethionine; MeSeCys, *Se*-methylselenocysteine; $HSe^-$, hydrogen selenide; SeCys, selenocysteine; MeSeH, methylselenol; XAS, X-ray absorption spectroscopy; XANES, X-ray absorption near-edge structure; EXAFS, extended X-ray absorption fine structure; XRF, X-ray fluorescence; PBS, phosphate-buffered saline; DMEM, Dulbecco's modified Eagle's medium; MTT, 3-(4,5-dimethylthiazol-2-yl)-2,5-diphenyltetrazolium bromide; SSRL, Stanford Synchrotron Radiation Lightsource; PCA, principal component analysis; APS, Advanced Photon Source; AS, Australian Synchrotron; CysSeSeCys, selenocystine; CysSSeCys, sulfoselenocystine.


Published on Web 01/24/2011

Studies of the speciation of Se in biological systems have relied largely on high-performance liquid chromatography coupled to inductively coupled plasma mass spectrometry, which is a method capable of accurately determining the concentration of major, minor, and trace components (*6*). However, this method requires extensive sample preparation that may itself alter the speciation of Se, thus confounding the results.

Synchrotron X-ray absorption and fluorescence methods are ideal probes for investigating the chemical speciation and distribution of elements heavier than Si, such as Se, in biological systems with minimal sample preparation. X-ray absorption spectroscopy (XAS) and X-ray fluorescence (XRF) microscopy have previously been used to study the speciation and distribution of Cr in human lung cancer cells (*14*) and the metabolism of As in human hepatoma cells (*15*). While there are no previous reports of Se K-edge XAS conducted on mammalian systems, Pickering et al. (*16*) have shown that the X-ray absorption spectra of several biologically relevant Se compounds are sufficiently different to allow the identification of Se species within a biological matrix. Herein we investigate the speciation and distribution of Se in A549 human lung carcinoma cells treated with selenoamino acids, SeMet and MeSeCys, using X-ray absorption near edge structure (XANES) spectroscopy, extended X-ray absorption fine structure (EXAFS) spectroscopy, and synchrotron radiation X-ray fluorescence (XRF) microscopy.

## EXPERIMENTAL PROCEDURES

*Materials*. Se-(methyl)selenocysteine hydrochloride (≥95%) and seleno-L-methionine (≥98%) were used as purchased from Sigma Aldrich. Solutions of the selenoamino acids in phosphate-buffered saline (PBS) (prepared using Milli-Q water) were prepared immediately before use.

*Cell Culture*. A549 human lung adenocarcinoma epithelial cells, originally purchased from the American Tissue Culture Collection, were a gift from A. Levina (The University of Sydney). Cells were cultured as monolayers in Dulbecco's modified Eagle's medium (DMEM) supplemented with fetal bovine serum (2%, v/v), L-glutamine (2 mM), an antibiotic/antimicotic mixture (100 mg/mL penicillin and 100 units/mL streptomycin), and nonessential amino acids (100 units/mL) at 310 K in a 5% $CO_2$-humidified incubator and were subcultured every 3−7 days.

*Cytotoxicity Assay*. Cytotoxicity was assessed using the MTT [3-(4,5-dimethylthiazol-2-yl)-2,5-diphenyltetrazolium bromide] assay (*17*). Briefly, cells were seeded at a density of $1 \times 10^4$ cells/well in a 96-well plate for 24 h at 310 K in a 5% $CO_2$-humidified incubator. Solutions of the selenoamino acids prepared by serial dilution in PBS (10 $\mu$L) were added to full-serum DMEM (100 $\mu$L). After treatment for 72 h, the cells were incubated with an MTT solution (0.25 mg/mL in serum-free DMEM) for 3 h. The MTT solution was then replaced with dimethyl sulfoxide (100 $\mu$L), and the absorbance of the formazan solution was measured at a wavelength of 560 nm using a microplate spectrophotometer (BMG Lab Tech Fluostar Galaxy). Cell viability was reported as the percentage absorbance relative to the control as a mean of three independent experiments (with eight replicates per experiment). $IC_{50}$ values were determined by curve-fitting plots of cell viability versus the log of Se compound concentration.

*Sample Preparation*. Bulk cell pellets from treated cultures were prepared for X-ray absorption spectroscopy. Cells were grown over 5 days to ~90% confluency in 75 $cm^2$ culture flasks in complete DMEM and were treated with SeMet (300 $\mu$L addition, yielding final concentrations of 100 and 200 $\mu$M), MeSeCys (300 $\mu$L addition, yielding final concentrations of 50 and 100 $\mu$M), or PBS (300 $\mu$L, as a vehicle-alone control) in fresh complete DMEM for 24 h. Cells were collected by gentle scraping and centrifugation. The supernatant was removed, and the cells were rinsed by resuspension in PBS (3 × 5 mL) and centrifugation before the pellet was collected and stored at 203 K and then vacuum-dried for 3 h.

Cells used in XRF imaging were grown on 1.5 mm × 1.5 mm × 500 nm silicon nitride windows (Silson) in six-well plates as described previously (*18*). Briefly, the plates were seeded at a density of $1.8 \times 10^5$ cells/well in complete DMEM and were incubated at 310 K in a 5% $CO_2$-humidified incubator for 24 h prior to treatment. Cells were treated with 50 $\mu$M SeMet or MeSeCys or PBS for 20 min (1 h PBS treatment) and 10 or 50 $\mu$M SeMet or MeSeCys or PBS for 24 h (as a vehicle-alone control) before the medium was removed and the cells were washed in PBS and fixed by being dipped in cold methanol (7 × 1 s). Samples were stored at 277 K.

*X-ray Absorption Spectroscopy and Data Analyses*. Se K-edge X-ray absorption spectra of the bulk cell pellets were recorded at the Stanford Synchrotron Radiation Lightsource (SSRL) on beamline 9-3. The X-ray beam was monochromated by reflection from a pair of Si(220) crystals. Harmonic rejection was achieved by setting the cutoff energy of a Rh-coated mirror to 15 keV. Cell pellets were compressed to approximately 3 mm in diameter, secured between Kapton tape, and cooled to ~10 K in a flowing He cryostat. A spectrum of MeSeCys, used as a model compound for XANES fitting, was obtained from a frozen 5 mM solution of MeSeCys in Milli-Q water. Spectra were recorded in fluorescence mode on a 30-element Ge detector array (Canberra) at 90° to the incident beam. The following energy ranges were used for XANES data collection: pre-edge region from 12425 to 12635 eV (10 eV steps), XANES region from 12635 to 12685 eV (0.25 eV steps), and postedge region from 12685 to 12872 eV (0.05 $Å^{-1}$ steps in *k*-space). EXAFS spectra were recorded over the following energy ranges: pre-edge region from 12435 to 12635 eV (10 eV steps), XANES region from 12635 to 12685 eV (0.25 eV steps), and EXAFS region from 12685 to 13443 eV (0.05 $Å^{-1}$ steps in *k*-space to 14 $Å^{-1}$). A hexagonal Se foil standard was used to calibrate the energy scale to the first peak of the first derivative of the Se edge (12658 eV).

Data analysis, including calibration, averaging, and background subtraction of all spectra and principal component analysis (PCA), and target and linear regression analyses of XANES spectra were performed using EXAFSPAK (G. N. George, Stanford Synchrotron Radiation Laboratory, Stanford, CA). Spectra of model Se compounds for target and linear regression analyses were provided by G. N. George (University of Saskatchewan, Saskatoon, SK) except for that of MeSeCys, which was obtained during these experiments.

*X-ray Fluorescence Imaging, μ-XANES Spectra, and Data Analyses*. XRF elemental distribution maps of single cells were recorded on beamline 2-ID-E at the Advanced Photon Source (APS), Argonne National Laboratory, and on the X-ray fluorescence microprobe (XFM) beamline (*19*) at the Australian Synchrotron (AS). At the APS, the beam was tuned to an incident energy of 13.0 keV using a beam splitting Si(220) monochromator and was focused to a diameter of 1 $\mu$m using a "high-flux" zone plate. The tail of the scatter peak from the incident 13.0 keV

beam does not significantly interfere with the Se Kα peak at ~11.2 keV (see Figure S1 of the Supporting Information). A single-element silicon drift energy dispersive detector (Vortex EX, SII Nanotechnology, Northridge, CA), at 90° to the incident beam, was used to collect the fluorescence signal for 1 s per spatial point from samples under a He atmosphere. At the AS, a monochromatic 13.0 keV X-ray beam was focused (to a spot size of ~1 μm × ~4 μm) using a zone plate, and the fluorescence signal was collected using a single-element silicon drift diode energy dispersive detector (Vortex EM, SII Nanotechnology), oriented at ~73 degrees to the incident beam for 3 s per spatial point. Individual cells were located using images obtained from an optical microscope positioned in the beamline downstream from the sample.

The fluorescence spectrum at each spatial point was fit to Gaussians, modified by the addition of a step function and a tailing function to describe mostly incomplete charge collection and other detector artifacts (*20*). For XRF images collected at the APS, two regions of interest corresponding to the whole cell (identified using optical images and the elemental distribution maps of P, S, Cl, K, and Zn) and nuclear regions (identified using optical images and regions of P and Zn colocalization) were selected. The integrated fluorescence spectra extracted from these regions were also fit with modified Gaussians to determine average elemental area densities (in units of micrograms per square centimeter). Quantification was performed by comparison to the corresponding measurements on the thin-film standards NBS-1832 and NBS-1833 from the National Bureau of Standards (Gaithersburg, MD). The analysis was performed using MAPS (*21*).

At the AS, several regions of high Se concentration in the XRF maps of Se distribution were selected for μ-XANES analysis. Data were collected over the following energy ranges: pre-edge region from 12500 to 12640 eV (10 eV steps), XANES region from 12640 to 12690 eV (0.5 eV steps), and postedge region from 12690 to 12900 eV (10 eV steps) with a dwell time of 1 s per point. The specimen was repositioned through the μ-XANES scan to track the motion of the X-ray focus with energy. The stability of the analyzed region of each cell was characterized at ~1 μm over the μ-XANES scan. A Se foil was used to calibrate the energy scale to the first peak of the first derivative of the elemental Se edge (12658 eV).

Data analysis, including the calibration, averaging, and background subtraction of μ-XANES spectra, was performed using EXAFSPAK. Fitting of multiple model compounds using multiple linear regression analysis was not attempted because of the high noise level of the spectra.

## RESULTS

MeSeCys ($IC_{50}$ = 100 ± 20 μM) exhibited a greater toxicity toward the A549 cells than SeMet ($IC_{50}$ = 500 ± 200 μM) following a 72 h treatment period. For samples prepared for XAS and XRF microscopy, cells were treated for up to 24 h with selenoamino acids at concentrations no higher than their 72 h $IC_{50}$ value.

Biologically relevant model Se compound spectra (Figure 1) exhibit a range of edge energies and peak shapes that vary with local Se environments. The broad peaks of the deprotonated selenides ($CysSe^-$ and $HSe^-$) are in stark contrast to the well-defined peaks of the diselenide and sulfoselenide (CysSeSeCys and CysSSeCys), which are, in turn, distinguishable from the less intense peaks of RSeR′ compounds (*16*). The Se K-edge X-ray absorption spectra of bulk A549 cell pellets treated with SeMet or

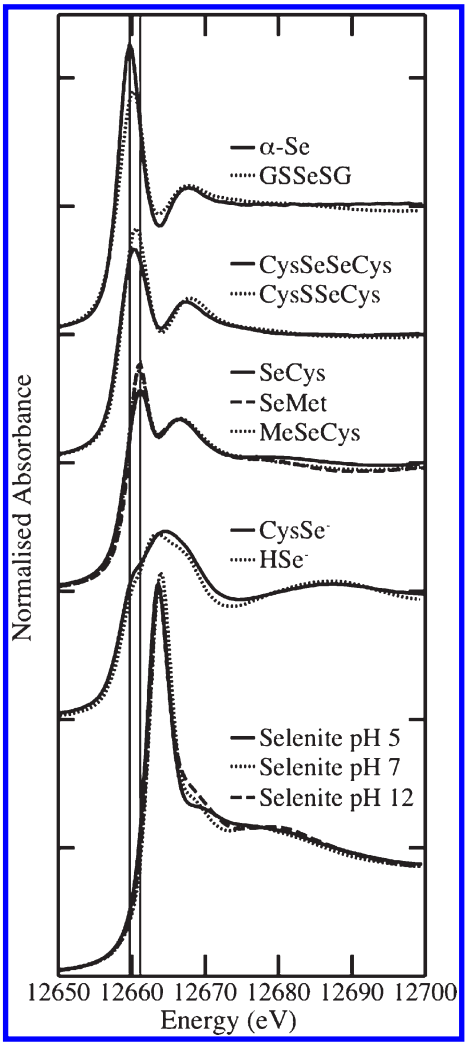


FIGURE 1: Se K-edge X-ray absorption near-edge spectra of Se model compounds.

MeSeCys for 24 h are presented in Figure 2. The spectra are very similar; however, the ratios of the high-energy to low-energy peak intensities in the SeMet-treated cell spectra (0.82) are lower than in the MeSeCys-treated cell spectra (0.84). PCA and target transformation indicated that SeCys, CysSeSeCys, MeSeCys, and SeMet were, of all the model compounds shown in Figure 1, the most likely components of the sample spectra. Results of linear combination fitting of the experimental spectra are listed in Table 1. All spectra were fit with large RSeH and RSeR′ components. A small, but noteworthy, difference between the SeMet- and MeSeCys-treated cell spectra (see Figure S2 of the Supporting Information for a difference plot) was highlighted by the fitting of a diselenide component (CysSeSeCys) to the MeSeCys-treated cell spectra, but not the SeMet-treated cell spectra.

The chemical speciation of Se in the SeMet-treated cell pellets was further investigated by EXAFS analysis (Figure 3). Table 2 shows the results of fitting one, two, or three C scatterers to the EXAFS spectra. Attempts at fitting other potential scatterers such as S and Se produced physically unrealistic values. Best fits to both spectra were obtained for two C scatterers with a C−Se bond length of 1.96 Å, which is consistent with the large RSeR′ component identified by XANES fitting. The interatomic distances and Debye−Waller factors of the Se−C bonds were identical at both treatment concentrations.

XRF elemental mapping of single 50 $\mu$M SeMet-treated A549 cells revealed a significant uptake of Se after 20 min, compared to control A549 cells (Table S1 of the Supporting Information), with Se distributed throughout the cell (Figure 4). In contrast, the Se contents of A549 vehicle-alone control cells were indistinguishable from background Se levels (Figure 5). SeMet treatment resulted in significant increases in intracellular Ca and Fe levels and decreases in K and Zn levels compared to control cells. At the same concentration and treatment time, the uptake of MeSeCys (Figure 6) was not significant for whole cells compared to control cells but was significant for the nuclear region, and significant differences were observed in the elemental area densities of P, S, K, Ca, Fe, Cu, and Zn for both the whole cell and nuclear region (defined as a region with a high degree of Zn and P localization) compared to control cells (Tables S1 and S2 of the Supporting Information). Interestingly, an efflux of Zn was observed in cells during both treatments, but the level of efflux was greater from the cytosol (Table S3 of the Supporting Information) than from the nuclear region as shown by the increase in the ratio of the nuclear to non-nuclear region elemental area densities from 1.9 in control cells to 3.0 and 2.8 in 50 $\mu$M SeMet-treated and 50 $\mu$M MeSeCys-treated cells, respectively (Table S4 of the Supporting Information).

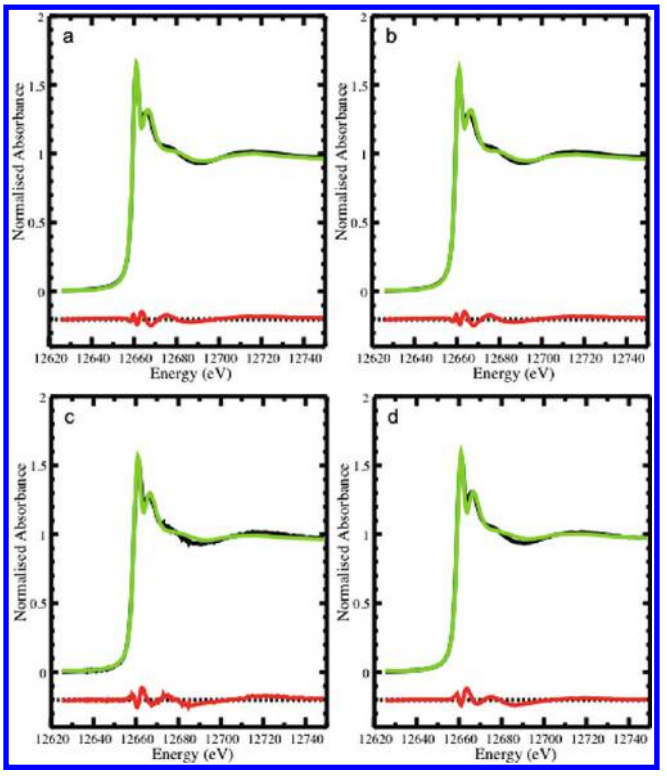


FIGURE 2: Se K-edge X-ray absorption near-edge spectra of A549 cells treated for 24 h with (a) 100 $\mu$M SeMet, (b) 200 $\mu$M SeMet, (c) 50 $\mu$M MeSeCys, or (d) 100 $\mu$M MeSeCys. The experimental spectra (black) were fit with a linear combination of spectra (green), and the residual is shown offset (red). The results of the linear combination analysis are listed in Table 1.

After 24 h, treatment with 10 $\mu$M SeMet led to a 70-fold increase in Se content, while treatment with 50 $\mu$M SeMet caused a 270-fold increase in Se content compared to that of control cells. A distinct region of high Se content was identified in the perinuclear region of cells treated with both 10 and 50 $\mu$M SeMet (Figures 7 and 8). The ratio of Se area densities of the nuclear to non-nuclear region was 2.1 in cells treated with both 10 and 50 $\mu$M SeMet compared to 1.1 in control cells. The increase is largely due to the inclusion of some of the perinuclear Se accumulation in the nuclear region of interest as a result of rendering a three-dimensional object in two dimensions. While some Se appears to have accumulated in the center of the nucleus, this is a thickness effect.

The elemental area densities of Se in cells treated with 10 and 50 $\mu$M SeMet were 45 and 65 times greater than in cells treated with the same concentrations of MeSeCys. SeMet treatment at both concentrations led to statistically significant increases in P, S, and Fe elemental area densities, while cells treated with 50 $\mu$M SeMet had significantly less K and more Ca and Cu than the control cells (Table S5 of the Supporting Information). Notably, the perinuclear Se accumulation was colocalized with a region of high S content (Figure 9).

MeSeCys-treated cells showed some uptake of Se after 24 h that was not statistically significant (1.5- and 4-fold greater than the levels observed in control cells for 10 and 50 $\mu$M treatments, respectively), yet significant changes were observed in the elemental area densities of other elements in these cells, including P, S, and Fe (Table S4 of the Supporting Information). In these cells, Se is barely distinguishable from background levels (Figure 10) and the distribution of Se appears homogeneous. Unlike SeMet-treated cells, there is no significant increase in the ratio of the nuclear to non-nuclear region Se area density after 24 h (Table S8 of the Supporting Information).

Figure 10 shows a representative $\mu$-XANES spectrum recorded in the perinuclear region of a cell treated with 50 $\mu$M SeMet for 24 h (Figure 11) and overlaid with XANES spectra of four model compounds. The low signal-to-noise ratio of the $\mu$-XANES spectra prevents the identification of components using multiple linear regression analysis. However, on the basis of the first peak positions of the sample spectra (from 12661.2 to 12661.4 eV), it is apparent that SeCys (12661.2 eV), SeMet (12661.5 eV), and MeSeCys (12661.4 eV) are likely to be major components. Despite the colocalization of S and Se evident in the elemental distribution maps, CysSeSeCys is not consistent with the measured spectra (Figure 12).

Table 1: Percent Se Species in A549 Cells Treated with Selenoamino Acids for 24 h, As Estimated by a Linear Combination of Model Compound Spectra

| | | percentage of component fitted | | | | | |
|---|---|---|---|---|---|---|---|
| treatment compound | concn ($\mu$M) | SeCys | CysSeSeCys | MeSeCys | SeMet | $N_{tot}$[b] | residual ($\times 10^{-3}$) |
| SeMet | 100 | 48(3)[a] | – | – | 49(2)[a] | 97 | 0.27 |
| SeMet | 200 | 61(2)[a] | – | – | 37(2)[a] | 98 | 0.31 |
| MeSeCys | 50 | 66(5)[a] | 13(1)[a] | 19(4)[a] | – | 98 | 0.54 |
| MeSeCys | 100 | 53(4)[a] | 20(1)[a] | 26(4)[a] | – | 99 | 0.46 |

[a]Values in parentheses are the estimated standard deviations derived from the diagonal elements of the covariance matrix and are a measure of precision. [b]$N_{tot}$ is the sum of the fractions.

## DISCUSSION

Linear combination fitting of standard Se spectra to XANES spectra revealed significant differences in the metabolism of SeMet and MeSeCys by A549 cells, despite the similar appearance of the spectra. Cells exposed to each of the Se compounds had a large RSeH component, but only MeSeCys-treated cells contained diselenides. The fitting of SeCys and SeMet components to the XANES spectra of SeMet-treated cells was supported by the fitting of two C scatterers to the EXAFS spectra of those cells. Unfortunately, the XAS signal of MeSeCys-treated cells was 20-fold lower than for SeMet-treated cells and, therefore, was too low for the collection of useful EXAFS spectra. As such, the presence of species containing a Se−Se bond in MeSeCys-treated cells could not be confirmed using EXAFS.

Despite the apparent similarity of the SeMet and MeSeCys model compound spectra (Figure 1), SeMet was fit to SeMet-treated cells, but not MeSeCys-treated cells, while the reverse was true for MeSeCys. A difference plot (Figure S2 of the Supporting Information) of the two model compounds shows that the spectra of SeMet and MeSeCys differ at the edge position and in the relative intensity of the main peak with respect to the edge jump, where differences in the spectra of the SeMet- and MeSeCys-treated cells also appear (Figure S2 of the Supporting Information). Nonetheless, the similarity of the SeMet and MeSeCys model compound spectra indicates that determination of their relative concentration by this method should be treated with some caution.

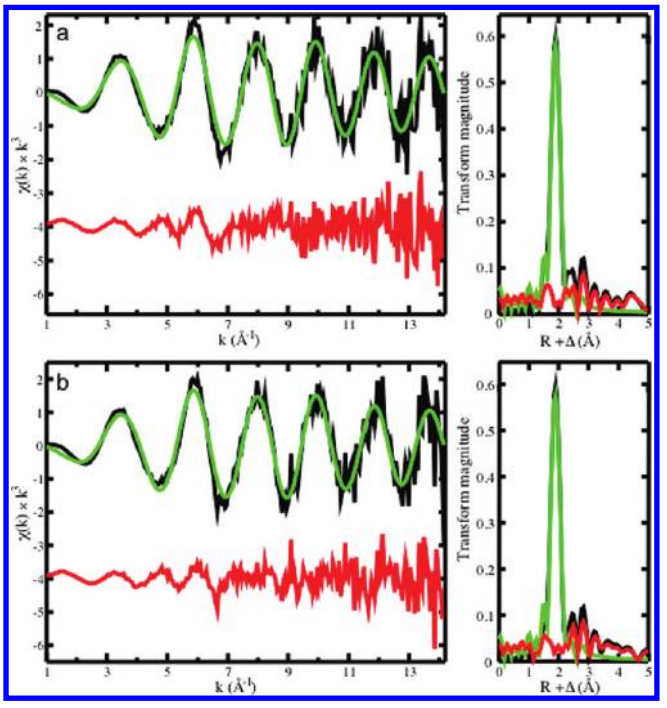


FIGURE 3: EXAFS spectra (left) and corresponding Fourier transforms (right) of A549 cells treated for 24 h with (a) 100 and (b) 200 $\mu$M SeMet showing experimental (black) and calculated (green) data with the residual shown offset (red). Fit parameters are listed in Table 2.

The fitting of a SeMet component to SeMet-treated cells and a MeSeCys component to MeSeCys-treated cells suggests that some SeMet and MeSeCys was not metabolized, although the SeMet component may also include SeMet adventitiously incorporated into proteins. The presence of species other than SeMet and MeSeCys in the fits indicates that both SeMet and MeSeCys were metabolized by A549 cells. This is in contrast to the findings of a recent study of Se metabolism in rat hepatocytes where SeMet and MeSeCys were recovered from cell lysates largely unchanged after a 4 h treatment (*22*).

The large SeCys component of both MeSeCys- and SeMet-treated cells may reflect the presence of SeCys in selenoproteins rather than free SeCys or selenols. While SeMet is known to be transformed to SeCys via the trans-selenation pathway (*23*), free SeCys (p$K_a$ = 5.24) (*24*) would exist with a deprotonated selenol at physiological pH, yet target transformation did not identify $CysSe^-$ as a component of the XANES spectra. In addition, selenols are redox active, and with a redox potential of −488 mV, free SeCys can be oxidized to CysSeSeCys under physiological conditions (*25*); however, a diselenide component was not fit to either of the SeMet-treated cell spectra. Thus, it is unlikely that the SeCys component identified in the spectra represents free SeCys. The environment within the folds of a protein can differ significantly from the intracellular environment, so the p$K_a$ of SeCys in selenoproteins may vary from that of free SeCys to such an extent that it exists in its selenol form.

The presence of a diselenide component in MeSeCys-treated cells may be due to the cleavage of MeSeCys by $\beta$-lyase to the active anticarcinogenic compound MeSeH ($MeSe^-$ at physiological pH), which has been shown to generate superoxide in an in vitro chemical assay (*26*). The presence of diselenides indicates that some oxidation of selenols has occurred, which could be due to the generation of reactive oxygen species by MeSeH. However, there is no direct evidence of this hypothesis as MeSeH was not part of the model compound library.

Unlike MeSeCys-treated cells, the presence of a diselenide was not indicated by fits to the XANES spectra of SeMet-treated cells, nor was Se identified as a backscatterer by EXAFS analysis. These results suggest SeMet treatment did not change the intracellular redox environment to the same extent as MeSeCys treatment, if at all. This difference between the Se speciation in

Table 2: Parameters Fit to EXAFS Spectra of Cells Treated with SeMet[a]

| concn ($\mu$M) | scatterer | coordination number $N$ | interatomic distance $R$ (Å) | Debye−Waller factor $\sigma^2$ (Å$^2$) | $-\Delta E_0$[b] (eV) | fit error[c] |
|---|---|---|---|---|---|---|
| 100 | C | 1 | 1.964(4)[d] | −0.0006(2)[d,e] | 10(2)[d] | 0.54 |
| 100 | C | 2 | 1.960(3)[d] | 0.0021(2)[d] | 12(1)[d] | 0.45 |
| 100 | C | 3 | 1.956(3)[d] | 0.0042(2)[d] | 13.0(0.9)[d] | 0.48 |
| 200 | C | 1 | 1.958(4)[d] | −0.0005(2)[d,e] | 11(2)[d] | 0.52 |
| 200 | C | 2 | 1.956(3)[d] | 0.0021(2)[d] | 12.4(0.9)[d] | 0.42 |
| 200 | C | 3 | 1.953(3)[d] | 0.0042(2)[d] | 13.6(0.8)[d] | 0.44 |

[a]The $k$ range was 1−14.2 Å$^{-1}$, and a scale factor ($S_0^2$) of 0.9 was used for all fits. [b]$\Delta E_0 = E_0 - 12658$ (eV), where $E_0$ is the threshold energy. [c]The fit error is defined as $[\sum k^6(\chi_{exp} - \chi_{calc})^2/\sum k^6\chi_{exp}^2]^{1/2}$. [d]Values in parentheses are the estimated standard deviations derived from the diagonal elements of the covariance matrix and are a measure of precision. [e]A negative Debye−Waller factor is not physically possible, and as such, fitting one C scatterer is not physically realistic.

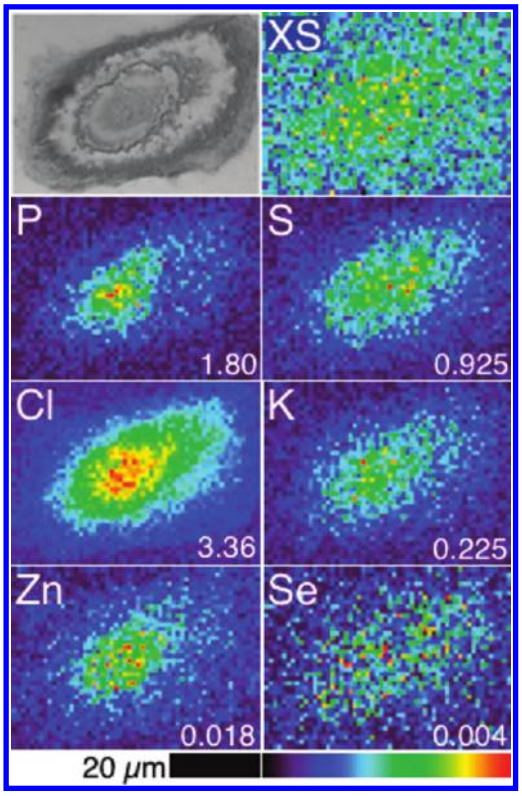


FIGURE 4: Optical micrograph (top left) and scattered X-ray (XS) and XRF elemental distribution maps of P, S, Cl, K, Zn, and Se of an A549 cell treated with 50 $\mu$M SeMet for 20 min. The maximal elemental area density (in micrograms per square centimeter) is given at the bottom right of each map.

MeSeCys- and SeMet-treated cells lends support to the hypothesis that adventitious incorporation of SeMet into proteins and its conversion to SeCys leave little SeMet available for cleavage by $\gamma$-lyase to the putative superoxide generator MeSeH, whereas MeSeCys is more readily available for cleavage to MeSeH.

That $HSe^-$ was not identified as a component of the spectra is notable because of its hypothesized role as an intracellular Se "pool". $HSe^-$ is thought to be produced by the cleavage of SeCys by $\beta$-lyase and by demethylation of MeSeH and would therefore be expected to be a metabolite of SeMet as well as MeSeCys. Despite its inclusion in the model compound library, it was not identified as a component of the XANES spectra by target transformation. Therefore, $HSe^-$ is probably not a significant chemical store of intracellular Se. This result is in keeping with the ready oxidation of $HSe^-$ by biological compounds such as disulfides and quinones (*27*), its rapid reaction with oxygen to form elemental Se, and the formation of Se−Se and Se−S bonds with selenols and thiols (*28*).

While the differences in chemical speciation between cells treated with SeMet and MeSeCys were significant, only small differences in the proportions of components were observed in Se speciation between two different treatment concentrations of the same compound. The similarity of the SeMet-treated cell spectra was underscored by the identical interatomic distances and Debye−Waller factors calculated from the EXAFS spectra of the cells treated with 100 and 200 $\mu$M SeMet.

The different metabolic pathways of SeMet and MeSeCys are highlighted by the differences in their uptake and distribution at the same treatment concentrations. Se was distributed throughout cells treated with SeMet but was particularly concentrated at

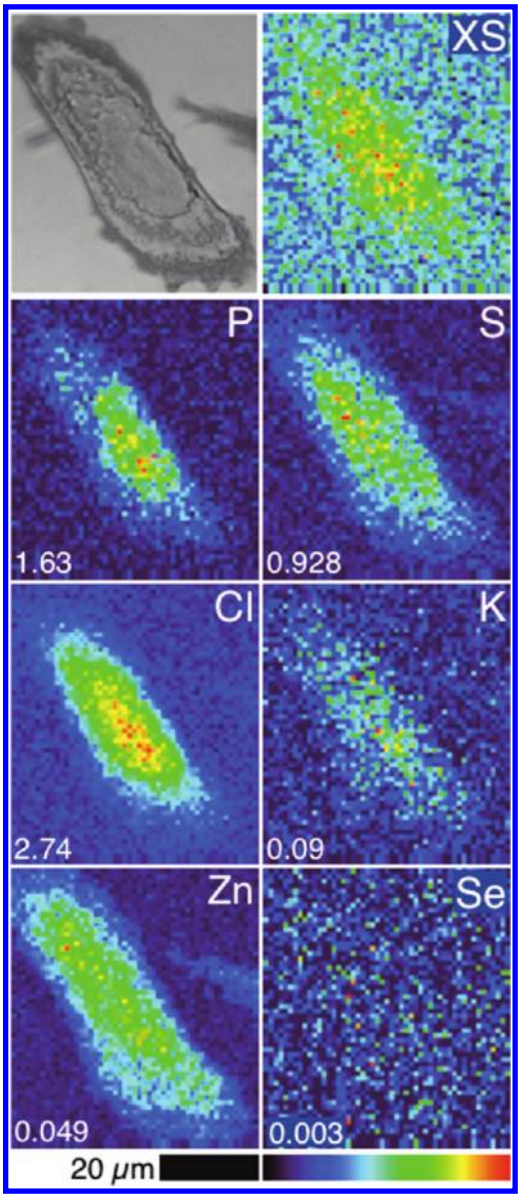


FIGURE 5: Optical micrograph (top left) and scattered X-ray (XS) and XRF elemental distribution maps of P, S, Cl, K, Zn, and Se of an A549 cell treated with PBS as a vehicle control for 1 h. The maximal elemental area density (in micrograms per square centimeter) is given at the bottom left of each map.

the edge of the nucleus in cells treated for 24 h with 10 and 50 $\mu$M SeMet. This phenomenon was not observed in the MeSeCys-treated cells, where the uptake of Se was much weaker than in SeMet-treated cells.

The localization of Se in the perinuclear region in SeMet-treated cells was a time- and concentration-dependent effect. Studies of the uptake of SeMet by erythroleukemia cells have shown that Se saturation occurred after 24 h in 10 $\mu$M SeMet-treated cells compared to 48 h in 50 $\mu$M SeMet-treated cells (*29*). Thus, the accumulation of SeMet at the edge of the cell nucleus may be related to the metabolism and storage of excess Se as it approaches saturation in the cell. While the region of Se accumulation is unidentified, the apparent compartmentalization suggests that SeMet has a specific biological activity. The proximity of the region to the nucleus leads to the possibility that the endoplasmic reticulum is the Se-accumulating organelle. Seven mammalian selenoproteins are known to reside in the endoplasmic reticulum, where membrane-bound or secreted

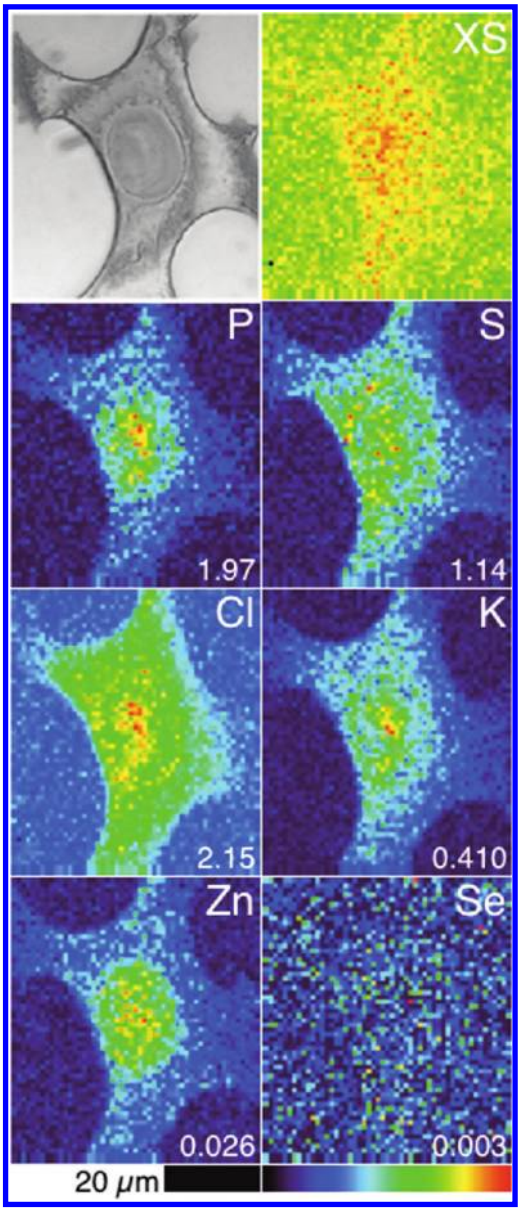


FIGURE 6: Optical micrograph (top left) and scattered X-ray (XS) and XRF elemental distribution maps of P, S, Cl, K, Zn, and Se of an A549 cell treated with 50 $\mu$M MeSeCys for 20 min. The maximal elemental area density (in micrograms per square centimeter) is given at the bottom right of each map.

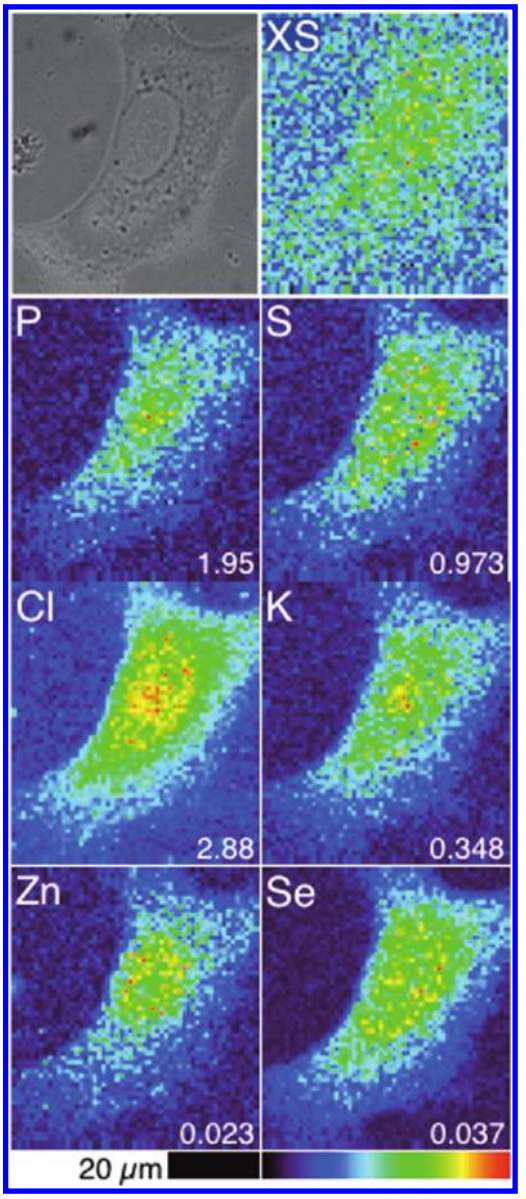


FIGURE 7: Optical micrograph (top left) and scattered X-ray (XS) and XRF elemental distribution maps of P, S, Cl, K, Zn, and Se of an A549 cell treated with 10 $\mu$M SeMet for 24 h. The maximal elemental area density (in micrograms per square centimeter) is given at the bottom right of each map.

proteins are also synthesized, and the high Se content in this region may reflect the utilization of SeMet or its metabolites for selenoprotein synthesis (*30*). The perinuclear localization may also reflect the nonspecific incorporation of SeMet in proteins in place of methionine, although we are not aware of methionine-rich proteins that would exhibit enhanced expression and localization in this region of the cell.

Se was colocalized with S in the perinuclear region, so the possibility that species containing Se−S bonds were present in this area was investigated using $\mu$-XANES spectroscopy. While no Se−S species was observed in the bulk XANES spectra, it could be argued that any Se−S species were too small a component of the entire cell to be identified by bulk XANES spectra and could be identified only by linear combination fitting of the $\mu$-XANES spectra. However, linear combination fitting could not be conducted as the signal-to-noise ratio was too low to resolve the energy of the second peak. Comparison of the $\mu$-XANES spectra recorded in the perinuclear region of two cells treated with 50 $\mu$M SeMet with components based on peak position and peak intensity ratios suggests that RSeR′ and RSeH species were the most likely components, as observed in the bulk XANES spectra. While the colocalization of Se and S in the cell may indicate a specific biological role of SeMet and it metabolites, it does not appear to reflect the presence of species containing Se−S bonds.

A difference in the uptake of SeMet and MeSeCys at both the 20 min and 24 h treatment times was observed. The increase in the Se content of cells treated for 20 min indicates that both SeMet and MeSeCys are quickly taken up and utilized by the cells, although the level of uptake of SeMet is greater than that of MeSeCys. Several amino acid transport systems have been shown to be involved in the transport of selenoamino acids, and the uptake of the selenoamino acids, including SeMet and MeSeCys, by intestinal and renal cells is considered to be dependent on the relative abundance of different amino acid transport systems in those cell lines (*31*). The disparity in SeMet and MeSeCys content

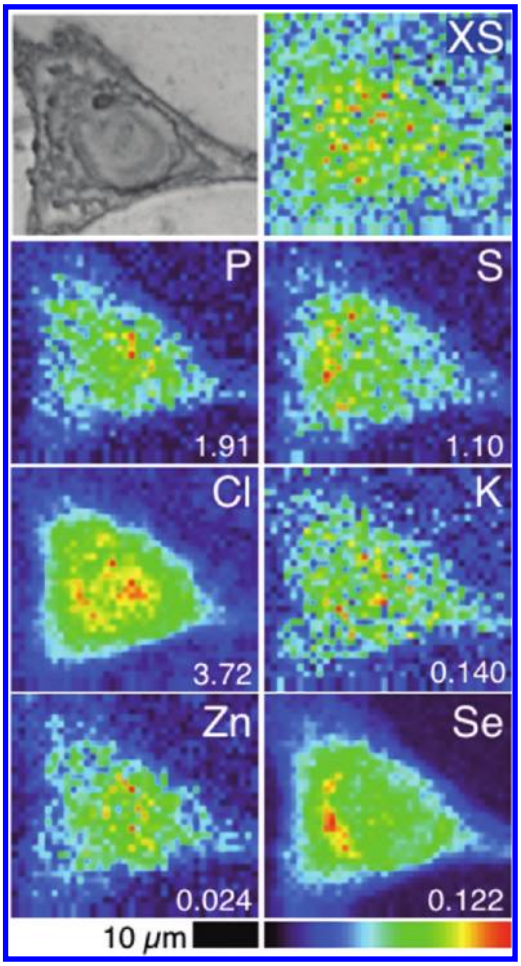


FIGURE 8: Optical micrograph (top left) and scattered X-ray (XS) and XRF elemental distribution maps of P, S, Cl, K, Zn, and Se of an A549 cell treated with 50 $\mu$M SeMet for 24 h. The maximal elemental area density (in micrograms per square centimeter) is given at the bottom right of each map.

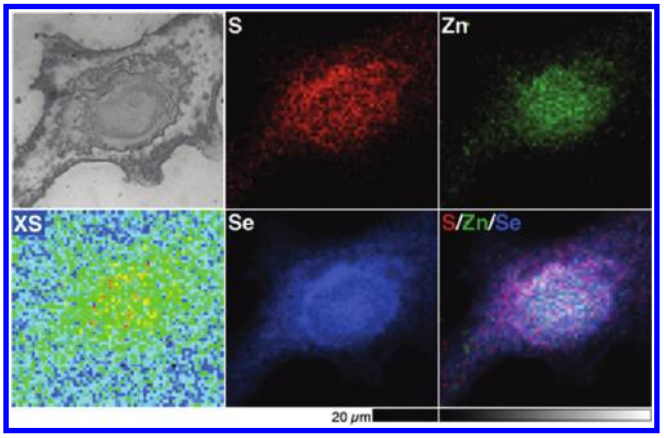


FIGURE 9: Optical micrograph (top left) and scattered X-ray (XS) and XRF elemental distribution maps of S, Zn, and Se of an A549 cell treated with 50 $\mu$M SeMet for 24 h. S (red), Zn (green), and Se (blue) maps are overlaid to show the colocalization of the elements (S/Zn/Se). Regions with high degrees of S and Se colocalization appear light pink in the S/Zn/Se overlay.

is even greater after 24 h where the Se content of 50 $\mu$M SeMet-treated cells is almost 70-fold higher than that of 50 $\mu$M MeSeCys-treated cells. The relative Se contents of the cells can also be approximated by the size of the XAS signal, and significantly, the maximal raw absorbance signal of cells treated with 100 $\mu$M SeMet

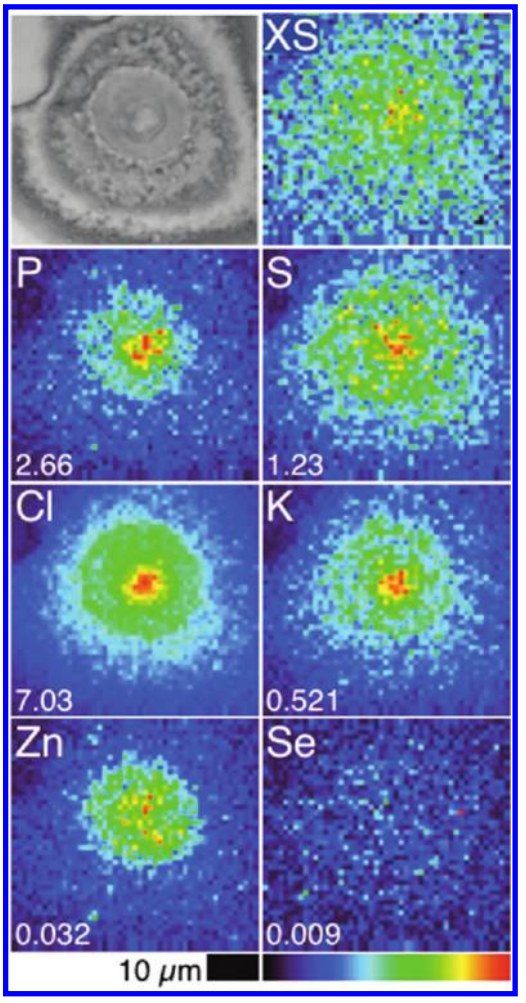


FIGURE 10: Optical micrograph (top left) and scattered X-ray (XS) and XRF elemental distribution maps of P, S, Cl, K, Zn, and Se of an A549 cell treated with 50 $\mu$M MeSeCys for 24 h. The maximal elemental area density (in micrograms per square centimeter) is given at the bottom left of each map.

for 24 h was only 20-fold greater than for cells treated with 100 $\mu$M MeSeCys for 24 h. The preparation of bulk and single cell samples differed only in that the PBS wash of the single cells was followed by a methanol wash. Methanol may strip Se from MeSeCys-treated cells but not SeMet-treated cells, resulting in the different relative Se contents of bulk and single cells treated with SeMet or MeSeCys for 24 h. This is further indirect evidence that the metabolism of the two selenoamino acids differs, with the MeSeCys converted into a more labile form in the cell.

While large disparities were observed in the intracellular Se contents of cells treated with the same concentrations of MeSeCys or SeMet for the same times, all selenoamino acid treatments caused significant changes to the intracellular contents of other major and trace elements. Interestingly, all treatments led to a significant increase in Fe content, and while there was an efflux of Zn after 20 min treatments that was more pronounced in the cytosol, Zn levels had returned to the same levels seen in the controls after 24 h. Perturbations in the levels of other elements were less uniform and appear to be dependent on treatment time, concentration, and treatment compound.

It is conceivable that the observed difference in the cellular distribution of selenium in cells treated with the two amino acids results from the differing abilities of the cells to absorb (or retain) the two species. Indeed, the relatively low concentration of Se

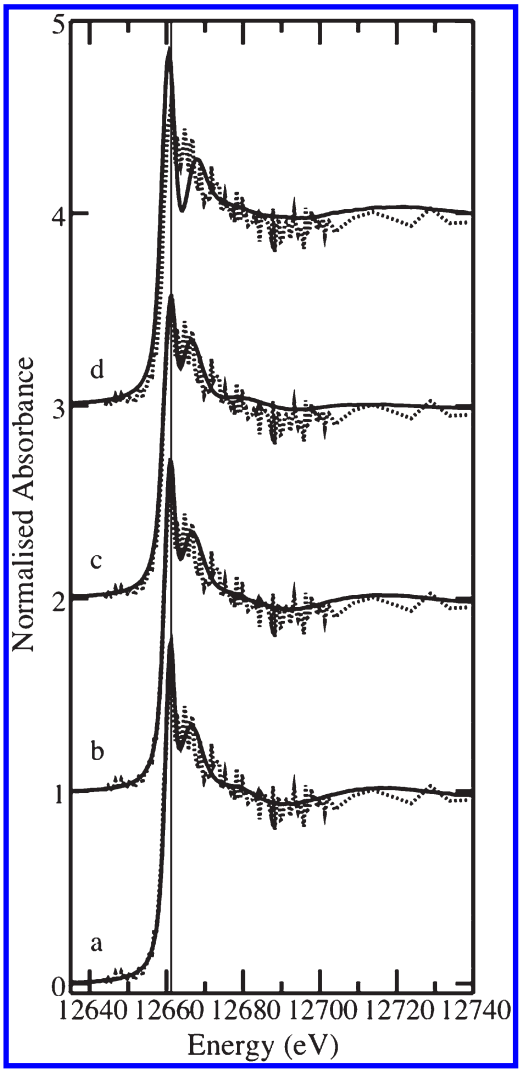


FIGURE 11: Se K-edge $\mu$-XANES spectrum in the perinuclear, high-Se and -S region of an A549 cell treated with 50 $\mu$M SeMet for 24 h (shown in Figure 10). The experimental spectrum (···) is overlaid with model compound spectra of (a) SeMet, (b) MeSeCys, (c) SeCys, and (d) CysSSeCys.

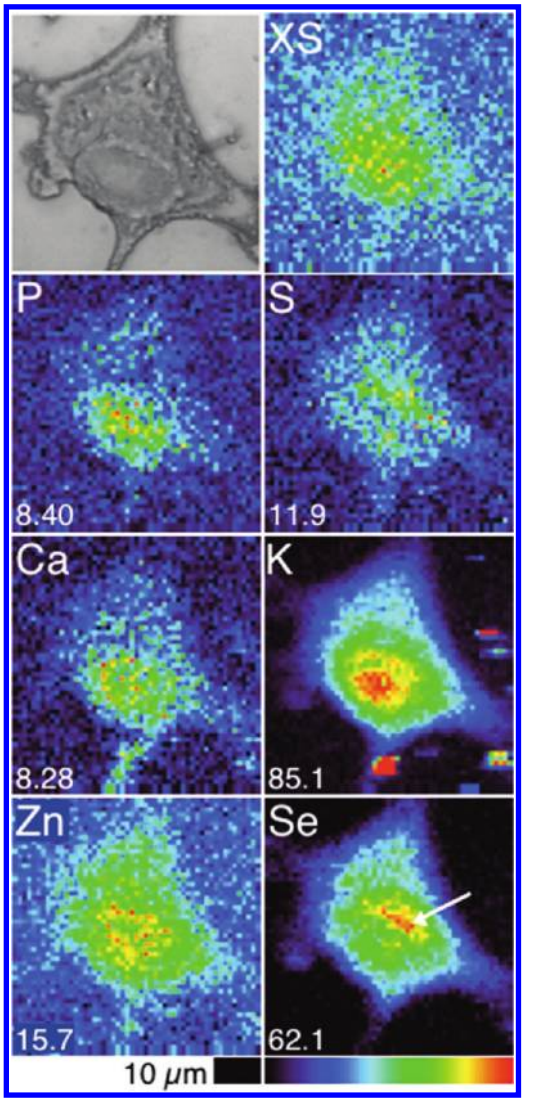


FIGURE 12: Optical micrograph (top left) and scattered X-ray (XS) and XRF elemental distribution maps of P, S, Cl, K, Zn, and Se of an A549 cell treated with 50 $\mu$M SeMet for 24 h. The maximal counts per second per pixel are given at the bottom left of each map. The arrow indicates the location where Se K-edge $\mu$-XANES was collected.

detected by XRF in MeSeCys-treated cells, combined with the variation in the observed uptake of the two amino acids, indicates that interpretation of the differing distributions should be performed with these limitations in mind. However, the observed differences in bulk Se speciation, and the different effect on the concentration of endogenous elements in the cells as a result of treatment with the two species, along with the observation that MeSeCys is more toxic than SeMet despite its lower level of uptake strongly support a distinct metabolism for these species in these cancer cells.

## CONCLUSION

Se XAS revealed that Se in cells treated with the selenoamino acids is largely found bound to C, which would be expected in SeMet and MeSeCys. However, while a RSeH component (possibly representing SeCys in selenoproteins) was identified in SeMet- and MeSeCys-treated cells, a diselenide component was identified in MeSeCys-treated cells, lending support to the hypothesis that while SeMet is adventitiously incorporated into proteins, MeSeCys is available for cleavage to MeSeH, a putative superoxide generator, which could produce the oxidizing conditions required for diselenide formation. $HSe^-$ was not identified as a component of any XANES spectra, which casts doubt on the long-held assumption that free selenide is a significant store of intracellular Se.

XRF microscopy revealed an accumulation of Se and S in the perinuclear region of SeMet-treated cells after 24 h, which was absent in MeSeCys-treated cells. While the reason for this accumulation has not been established, the Se in this region appears to be C-bound and not S-bound. SeMet and MeSeCys treatments caused perturbations in elemental area densities of major and other trace biological elements. The low Se contents of the MeSeCys-treated cells compared to the SeMet-treated cells after 20 min and 24 h treatments are a result of a lower level of uptake of MeSeCys that has most likely been exacerbated by the stripping of labile Se species from MeSeCys-treated cells by methanol fixation.

Taken together, the results of the X-ray absorption and fluorescence studies show that the selenoamino acids, SeMet and MeSeCys, follow different metabolic pathways that result in subtle but important differences in speciation in cancer cells and very dissimilar intracellular distributions. These results show the

utility of XAS and XRF microscopy in investigating the speciation and distribution of Se in human cancer cells with limited sample preparation.

## ACKNOWLEDGMENT

A549 cells were a gift from Aviva Levina (The University of Sydney). Graham N. George (University of Saskatchewan) provided Se K-edge X-ray absorption spectra of model Se compounds. Use of the Advanced Photon Source at Argonne National Laboratory was supported by the U.S. Department of Energy, Office of Science, Office of Basic Energy Sciences, under Contract DE-AC02-06CH11357. Parts of this research were conducted at the Stanford Synchrotron Radiation Labnoratory, a national user facility operated by Stanford University on behalf of the U.S. Department of Energy, Office of Basic Energy Sciences, and at the X-ray Fluorescence Microprobe beamline at the Australian Synchrotron.

## SUPPORTING INFORMATION AVAILABLE

Representative XRF spectrum of a whole cell treated with 50 $\mu$M SeMet for 24 h (Figure S1), difference between the spectra of cells treated with 100 $\mu$M SeMet or 100 $\mu$M MeSeCys (Figure S2), representative XRF image of a control cell at 24 h (Figure S3), and elemental area densities of cells imaged using XRF microscopy (Tables S1−S8). This material is available free of charge via the Internet at http://pubs.acs.org.

## REFERENCES

1. Clark, L. C., Combs, G. F., Turnbull, B. W., Slate, E. H., Chalker, D. K., Chow, J., Davis, L. S., Glover, R. A., Graham, G. F., Gross, E. G., Krongrad, A., Lesher, J. L., Park, H. K., Sanders, B. B., Smith, C. L., and Taylor, J. R. (1996) Effects of selenium supplementation for cancer prevention in patients with carcinoma of the skin. A randomized controlled trial. Nutritional Prevention of Cancer Study Group. *JAMA, J. Am. Med. Assoc. 276*, 1957–1963.
2. Duffield-Lillico, A. J., Dalkin, B. L., Reid, M. E., Turnbull, B. W., Slate, E. H., Jacobs, E. T., Marshall, J. R., and Clark, L. C. (2003) Selenium supplementation, baseline plasma selenium status and incidence of prostate cancer: An analysis of the complete treatment period of the Nutritional Prevention of Cancer Trial. *BJU Int. 91*, 608–612.
3. Lippman, S. M., Klein, E. A., Goodman, P. J., Lucia, M. S., Thompson, I. M., Ford, L. G., Parnes, H. L., Minasian, L. M., Gaziano, J. M., Hartline, J. A., Parsons, J. K., Bearden, J. D., Crawford, E. D., Goodman, G. E., Claudio, J., Winquist, E., Cook, E. D., Karp, D. D., Walther, P., Lieber, M. M., Kristal, A. R., Darke, A. K., Arnold, K. B., Ganz, P. A., Santella, R. M., Albanes, D., Taylor, P. R., Probstfield, J. L., Jagpal, T. J., Crowley, J. J., Meyskens, F. L., Baker, L. H., and Coltman, C. A. (2009) Effect of selenium and vitamin E on risk of prostate cancer and other cancers: The Selenium and Vitamin E Cancer Prevention Trial (SELECT). *JAMA, J. Am. Med. Assoc. 301*, 39–51.
4. Larsen, E. H., Hansen, M., Paulin, H., Moesgaard, S., Reid, M., and Rayman, M. (2004) Speciation and bioavailability of selenium in yeast-based intervention agents used in cancer chemoprevention studies. *J. AOAC Int. 87*, 225–232.
5. Ip, C., and Ganther, H. E. (1990) Activity of methylated forms of selenium in cancer prevention. *Cancer Res. 50*, 1206–1211.
6. Gammelgaard, B., Gabel-Jensen, C., Stürup, S., and Hansen, H. R. (2008) Complementary use of molecular and element-specific mass spectrometry for identification of selenium compounds related to human selenium metabolism. *Anal. Bioanal. Chem. 390*, 1691–1706.
7. Soriano-Garcia, M. (2004) Organoselenium compounds as potential therapeutic and chemopreventive agents: A review. *Curr. Med. Chem. 11*, 1657–1669.
8. Ganther, H. E. (1986) Pathways of selenium metabolism including respiratory excretory products. *J. Am. Coll. Toxicol. 5*, 1–5.
9. Ip, C., Hayes, C., Budnick, R. M., and Ganther, H. E. (1991) Chemical form of selenium, critical metabolites, and cancer prevention. *Cancer Res. 51*, 595–600.
10. Jiang, C., Jiang, W. Q., Ip, C., Ganther, H. E., and Lu, J. (1999) Selenium-induced inhibition of angiogenesis in mammary cancer at chemopreventive levels of intake. *Mol. Carcinog. 26*, 213–225.
11. Esaki, N., Nakamura, T., Tanaka, H., and Soda, K. (1982) Selenocysteine lyase, a novel enzyme that specifically acts on selenocysteine. Mammalian distribution and purification and properties of pig liver enzyme. *J. Biol. Chem. 257*, 4386–4391.
12. Okuno, T., Kubota, T., Kuroda, T., Ueno, H., and Nakamuro, K. (2001) Contribution of enzymic $\alpha,\gamma$-elimination reaction in detoxification pathway of selenomethionine in mouse liver. *Toxicol. Appl. Pharmacol. 176*, 18–23.
13. Ganther, H. E., and Lawrence, J. R. (1997) Chemical transformations of selenium in living organisms. Improved forms of selenium for cancer prevention. *Tetrahedron 53*, 12299–12310.
14. Harris, H. H., Levina, A., Dillon, C. T., Mulyani, I., Lai, B., Cai, Z., and Lay, P. A. (2005) Time-dependent uptake, distribution and biotransformation of chromium(VI) in individual and bulk human lung cells: Application of synchrotron radiation techniques. *J. Biol. Inorg. Chem. 10*, 105–118.
15. Munro, K. L., Mariana, A., Klavins, A. I., Foster, A. J., Lai, B., Vogt, S., Cai, Z., Harris, H. H., and Dillon, C. T. (2008) Microprobe XRF mapping and XAS investigations of the intracellular metabolism of arsenic for understanding arsenic-induced toxicity. *Chem. Res. Toxicol. 21*, 1760–1769.
16. Pickering, I. J., George, G. N., Van Fleet-Stalder, V., Chasteen, T. G., and Prince, R. C. (1999) X-ray absorption spectroscopy of selenium-containing amino acids. *J. Biol. Inorg. Chem. 4*, 791–794.
17. Mosmann, T. (1983) Rapid colorimetric assay for cellular growth and survival: Application to proliferation and cytotoxicity assays. *J. Immunol. Methods 65*, 55–63.
18. Carter, E. A., Rayner, B. S., McLeod, A. I., Wu, L. E., Marshall, C. P., Levina, A., Aitken, J. B., Witting, P. K., Lai, B., Cai, Z. H., Vogt, S., Lee, Y. C., Chen, C. I., Tobin, M. J., Harris, H. H., and Lay, P. A. (2010) Silicon nitride as a versatile growth substrate for microspectroscopic imaging and mapping of individual cells. *Mol. BioSyst. 6*, 1316–1322.
19. Paterson, D. J., Boldeman, J. W., Cohen, D. D., and Ryan, C. G. (2007) Microspectroscopy beamline at the Australian synchrotron. *AIP Conf. Proc. 879*, 864–867.
20. Espen, P. V. (2002) Spectrum Evaluation. In Handbook of X-Ray Spectrometry: Second Edition: Revised and Expanded (Grieken, R. E. V., and Markowicz, A. A., Eds.) Marcel Dekker, Inc., New York.
21. Vogt, S. (2003) MAPS: A set of software tools for analysis and visualization of 3D X-ray fluorescence data sets. *J. Phys. IV 104*, 635–638.
22. Gabel-Jensen, C., and Gammelgaard, B. (2010) Selenium metabolism in hepatocytes incubated with selenite, selenate, selenomethionine, Se-methylselenocysteine and methylseleninc acid and analysed by LC-ICP-MS. *J. Anal. At. Spectrom. 25*, 414–418.
23. Esaki, N., Nakamura, T., Tanaka, H., Suzuki, T., Morino, Y., and Soda, K. (1981) Enzymatic synthesis of selenocysteine in rat liver. *Biochemistry 20*, 4492–4496.
24. Huber, R. E., and Criddle, R. S. (1967) Comparison of the chemical properties of selenocysteine and selenocystine with their sulfur analogs. *Arch. Biochem. Biophys. 122*, 164–173.
25. Jacob, C., Giles, G., Giles, N., and Sies, H. (2003) Sulfur and selenium: The role of oxidation state in protein structure and function. *Angew. Chem., Int. Ed. 42*, 4742–4758.
26. Spallholz, J. E., Shriver, B. J., and Reid, T. W. (2001) Dimethyldiselenide and methylseleninic acid generate superoxide in an in vitro chemiluminescence assay in the presence of glutathione: Implications for the anticarcinogenic activity of L-selenomethionine and L-Se-methylselenocysteine. *Nutr. Cancer 40*, 34–41.
27. Nuttall, K. L., and Allen, F. S. (1984) Redox reactions of hydrogen selenide ion. *Inorg. Chim. Acta 92*, 33–36.
28. Spallholz, J. E. (1994) On the nature of selenium toxicity and carcinostatic activity. *Free Radical Biol. Med. 17*, 45–64.
29. Frisk, P., Yaqob, A., Nilsson, K., Carlsson, J., and Lindh, U. (2000) Uptake and retention of selenite and selenomethionine in cultured K-562 cells. *BioMetals 13*, 209–215.
30. Shchedrina, V. A., Zhang, Y., Labunskyy, V. M., Hatfield, D. L., and Gladyshev, V. N. (2010) Structure-function relationships, physiological roles and evolution of mammalian ER-resident selenoproteins. *Antioxid. Redox Signaling 12*, 839–849.
31. Nickel, A., Kottra, G., Schmidt, G., Danier, J., Hofmann, T., and Daniel, H. (2009) Characteristics of transport of selenoamino acids by epithelial amino acid transporters. *Chem.-Biol. Interact. 177*, 234–241.